Astronomy & Astrophysics manuscript no. article
(DOI: will be inserted by hand later)
April 18, 2005

Dust Distribution during Reionization

Erik Elfgren[1], François-Xavier Désert[2], Bruno Guiderdoni[3], and Eric Hivon[4]

[1] Department of Physics, Luleå University of Technology, SE-971 87 Luleå, Sweden
[2] Laboratoire d'Astrophysique, Observatoire de Grenoble, BP 53, 414 rue de la piscine, 38041 Grenoble Cedex 9, France
[3] Observatoire de Lyon, 9, avenue Charles Andr, 69561 St-Genis Laval Cedex, France
[4] IPAC/Caltech, Mail Code 100-22, 770 S. Wilson Av., Pasadena, CA 91125, USA

Received ¡date¿ / Accepted ¡date¿

Abstract. The dust produced by the first generation of stars will block the Cosmic Microwave Background to some extent. In order to evaluate this, we calculate the power spectrum of the dust and show that this dust might be detectable with the Planck satellite at small angular scales ($\ell \gtrsim 1000$). The power spectrum of the dust is compared with errors of Planck and is found to noticeable for certain values of dust lifetime and dust production rates.

Key words. Dust – CMB – Reionization – Power spectrum

1. Introduction

The importance of the Cosmic Microwave Background (CMB) as a cosmological tool has been demonstrated thoroughly during the last few years. It has been used to evaluate the age of the universe, the Hubble parameter, the baryon content, the flatness and the optical depth of the reionization, Bennett et al. (2003); the non-Gaussianity of the primary fluctuations, Komatsu et al. (2003); the Sunyaev-Zeldovich fluctuations from the first stars, Oh et al. (2003); the primordial magnetic fields, Subramanian et al. (2003); the spatial curvature of the universe, Efstathiou (2003); the formation of population III stars, Cen (2003); and the neutrino masses, Hannestad (2003).

However, in order to interpret the CMB signal correctly, its foreground must also be well known.

In this paper we focus on one particular aspect of the foreground of the CMB: the primordial dust. This dust was created during the reionization period in the first generation of stars and was then ejected into the interstellar medium (ISM). The dust will therefore partly block the path of the CMB photons and slightly deform the spectrum. As we have shown in an earlier paper Elfgren & Désert (2004), this dust has a characteristic spectrum proportional to a primary anisotropy (ΔT) spectrum times the frequency squared. The dust spectrum was shown to be lower than the CMB by roughly two orders of magnitude because the heating from the stars is significantly less than that of the CMB at the time.

Nevertheless, the dust will also have a characteristic spatial distribution which could be used to identify its signal. The objective of this paper is to determine this distribution and its impact on different measurements of the CMB. Of particular interest is the Planck satellite mission, but also other instruments, like MAMBO and BLAST could be interesting. The spatial distribution is estimated from the GalICS (Galaxies In Cosmological Simulations) N-body simulations of dark matter, which are described in more detail in section 2. The dust distribution is then combined with the intensity of the dust emission as calculated in Elfgren & Désert (2004), and this is integrated along the line of sight. The resulting power spectrum is then plotted in terms of the spherical harmonics C_ℓ and compared with detection limits of Planck.

In our model, we assume a ΛCDM universe with $\Omega_{tot} = \Omega_m + \Omega_\Lambda = 1$, where $\Omega_m = \Omega_b + \Omega_{DM} = 0.133/h^2$, $\Omega_b = 0.0226/h^2$ and $h = 0.72$ as advocated by WMAP, Spergel et al. (2003), using WMAP data in combination with large scale structure observations (2dFGRS + Lyman α).

2. Dark Matter Simulations

The distribution of dark matter in the universe was calculated using the GalICS program. The cosmological N-body simulation we refer to throughout this paper was done using the parallel tree-code developed by Ninin (1999). The power spectrum was set in agreement with Eke et al. (1996): $\sigma_8 = 0.88$, and the Dark Matter (DM) density field was calculated from z=35.59 to z=0, outputting 100 snapshots spaced logarithmically in the expansion factor.

GalICS is a hybrid model for hierarchical galaxy formation studies, combining the outputs of large cosmological N-body simulations with simple, semi-analytic recipes to describe the fate of the baryons within dark matter halos. The simulations produce a detailed merging tree for the dark matter hales, including complete knowledge of the statistical properties arising from the gravitational forces.

Send offprint requests to: Erik Elfgren, e-mail: elf@ludd.luth.se

The basic principle of the simulations is to randomly distribute a number of dark matter particles N^3 with mass $M_{\rm DM}$ in a box of size L^3. Then, as time passes, the particles interact gravitationally, clumping together and forming structures. The clumps of Dark Matter are called halos and in our simulation we require at least 5 particles to clump together before we call it a halo. There are supposed to be no other forces present than the gravitation and the boundary conditions are assumed to be periodic.

In the simulations we used, the side of the box of the simulation is $L = 100h^{-1}$ Mpc and the number of particles are 256^3 which implies a particle mass of $\sim 5.51 \times 10^9 h^{-1} M_\odot$. Furthermore, the cosmological parameters were $\Omega_\Lambda = 2/3$, $\Omega_m = 1/3$ and $h = 2/3$. Between the assumed initial dust formation at $z \sim 15$ and the end of this epoch in the universe at $z \sim 5$, there are 51 snapshots. In each snapshot a friend-of-friend algorithm was used to identify virialized groups of at least five DM particles. The number of particles have been set low in order to produce halos already at $z = 14.7$.

In order to make a correct large-scale prediction of the distribution of the Dark Matter and therefore the dust, the size of the box would have to be of Hubble size, i.e. 3000 Mpc. However, increasing the size of the box and maintaining the same number of particles would mean that we loose in mass resolution, which is not acceptable if we want to reproduce a fairly realistic scenario of the evolution of the universe.

There is another way to achieve the desired size of the simulation without loosing in detail or making huge simulations. This method is called MoMaF (Mock Map Facility) and is described in detail in Blaizot et al. (2003). The basic principle is to use the same box, but at different stages in time and thus a cone of the line of sight can be established. In order to avoid replication effects, the periodic box is randomly rotated for each time-step. This means that there will be loss of correlation information on the edges of the box, since those parts will be gravitationally disconnected from the adjacent box. Fortunately, this loss will only be of the order of 10% as shown in Blaizot et al. (2003).

2.1. Validity of Simulation

The distribution of galaxies resulting from this GalICS simulation has been compared with the 2dS Colless et al. (2001) and the Sloan Digital Sky Survey Szapudi et al. (2001) and found to be realistic on the angular scales of $3' \lesssim \theta \lesssim 30'$, see Blaizot et al. (2003). The discrepancy in the spatial correlation function for other values of θ can be explained by the limits of the numerical simulation. Obviously, any information on scales larger than the size of the box is not reliable. Since the simulation gives reasonable predictions of the matter distributions today, it seems likely that it is also valid at higher z when the early dust is produced.

3. Model

Since very little is known about the actual distribution of the dust throughout the universe at this time, we simply assume that the dust distribution follows the dark matter distribution.

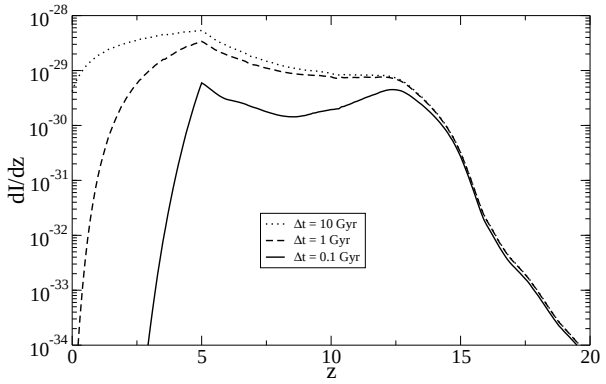

Fig. 1. Intensity contribution from the dust per time-step z.

We propose two different ways for this to happen and explore these. The first is to let the dust be proportional to the dark matter halos, the second is to make a hydrodynamical smoothing of the dark matter density field and set the dust density proportional to this density. In both cases we put

$$\rho_{dust}(\boldsymbol{r}, z) \propto \rho_{DM}(\boldsymbol{r}, z), \tag{1}$$

where ρ_{DM} represents either the Halo method or the Smoothing method density. We will focus on the Halo method since it is more likely that the dust will have formed in galaxies and halos than that it will have formed anywhere that there is dark matter.

In order to estimate the measured intensity, we need to do this distribution in terms of the intensity from the dust emission. In our previous paper, Elfgren & Désert (2004), we calculated the intensity as a function of redshift, supposing that none of the light emitted from the stars is absorbed. This is close enough to the truth since there are more than 100 ionizing photons produced per baryon. The result is plotted in Fig. 1.

In our present model, we put the spatial distribution of the dust intensity to

$$\frac{dI}{dz}(\boldsymbol{r}, z) = dI(z) \cdot \frac{\rho_{DM}(\boldsymbol{r}, z)}{\langle \rho_{DM} \rangle (z)}. \tag{2}$$

where $dI(z)$ is the dust intensity as measured at $z = 0$ and $\langle \rho_{DM} \rangle (z)$ is the mean Dark Matter density at redshift z. The MoMaF method (section 2) is then used to project the emitted intensity from the dust on a 45'×45' patch along the line of sight. The contribution from each simulated box is added and the integrated dust intensity is calculated.

For $z > 2.3$, the time-steps are smaller than the size of the box and each box overlap with the next box along the line of sight. However, for $z < 2.3$ the time-steps were simulated too far apart and when we pile the boxes, there will be a small part of the line of sight that will not be covered. Fortunately, this is of little consequence since the dust intensity is so low at this time. Each box is divided into a grid according to the resolution that we wish to test. For Planck this means a grid that is 9×9 pixels, for SCUBA 45×45 pixels.

To check the resulting intensity image, we have calculated its $\sum dI_{x,y}/N^2_{pix}$, where $dI_{x,y}$ is the observed intensity on pixel x, y and N^2_{pix} is the number of pixels, and found it to be equal to $\int dI(z)dz$ to within a few per cent.

4. Results and Discussion

As described above, the MoMaF technique produces an image of the line of sight. This image represents the patch of the sky covered by the box, 150 co-moving Mpc^2 which translates to $\sim$ 45' and is apodized (smoothed on the edges), so as to avoid artifacts on the edges. Thereafter the image is Fourier transformed into frequency space P_k. In order to convert this spectrum into spherical harmonics correlation function we apply the following transformation:

$$\ell = k2\pi/\theta, \quad (3)$$

$$C_\ell = \theta^2 C_k, \quad (4)$$

where θ is the size in radians of the box being analyzed. These C_ℓ are then calculated in units of $[\mu K^2/B_\nu(T_{CMB})]$ at a frequency ν = 353 GHz, which is one of the nine Planck frequency channels. As found in Elfgren & Désert (2004), the intensity is proportional to the frequency squared which means that the power spectrum from the dust at a frequency ν will be

$$C_\ell(\nu) = C_\ell(353\ \mathrm{GHz}) \cdot \left(\frac{\nu}{353\ \mathrm{GHz}}\right)^4. \quad (5)$$

In order to estimate an average power spectrum, 400 such images were generated and the C_ℓ were averaged of these. For comparison, we also tried to paste all these images together and calculate the C_ℓ for this (180×180 pixels) image. The result was very similar to the average C_ℓ. To validate our results, we have also calculated the r.m.s. of the images and compared with $\sum_\ell \frac{2\ell+1}{4\pi} C_\ell$ and found them to be compatible. The resulting power spectra can be seen in Fig. 2. As described in Elfgren & Désert (2004), the lifetime of these dust particles is a largely unknown factor and we plot three different lifetimes, 0.1, 1, 10 Gyrs. Furthermore, the intensity is proportional to the fraction of the formed metals that actually end up as dust, which we assumed to be f_d = 0.3. This means that the intensity $C_\ell(f_d) = C_\ell(f_d = 0.3) \cdot f_d^2$. We note that there is only a small difference between dust lifetimes of 10 Gyrs and 1 Gyr, while the 0.1 Gyr is lower by a factor four. The lowest curve in the figure represents the hydrodynamical smoothing method of distributing the dust for a dust lifetime of 1 Gyr. Naturally, it is significantly lower than the corresponding Halo method C_ℓ:s because the DM halos will be much more grainy (especially early in the history) than the smoothed DM field. The difference between the two methods is a factor of $\sim$ 10 but they do not have exactly the same form.

The dust frequency spectrum will be distinctly different from that of other sources in the same frequency range. As shown in Elfgren & Désert (2004), it will be $\propto \nu^2$. We compare this spectrum with that of the CMB $\Delta T/T$ and that of galactic dust, T=17 K, Boulanger et al. (1996). In order to focus on the forms of the spectra, we normalize the three curves to one at

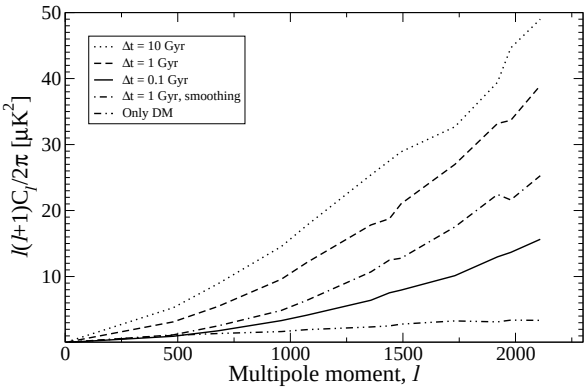

Fig. 2. Dust power spectrum at 353 GHz for a map 45'×45' and Planck resolution 5' for three different lifetimes for the dust particles, 0.1, 1, 10 Gyrs, with a solid, dashed and dotted line respectively. The dash-dash-dot line respresents the normalized correlation for the DM halos only without dust. The DM smoothing method for a dust lifetime of 1 Gyr is the dot-dot-dash line. We note that the DM smoothing method gives correlations that are approximately a factor ten lower than the DM halo method. Also, the form is not quite the same.

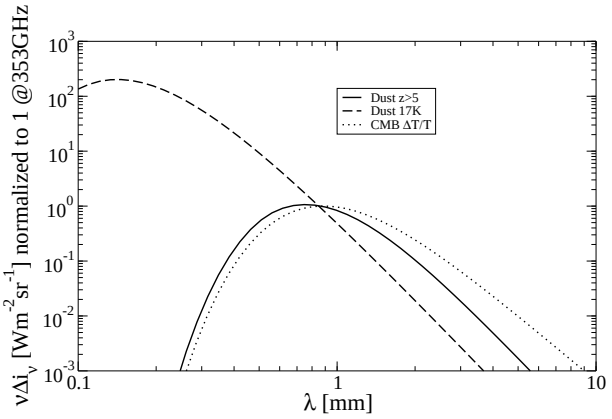

Fig. 3. The form of the early dust spectrum compared to the form of galactic dust (with a temperature of 17K) and the CMB. The curves have been normalized to 1 at 353 GHz. We see that the early dust has a special spectral signature.

ν = 353 GHz. The result is presented in Fig. 3. In case of a weak dust signal, this frequency signature could help us identify the signal by component separation spectral methods.

4.1. Detection with Planck?

The Planck satellite, due for launch in 2007, will have an angular resolution of $\sim$ 5' and will cover the whole sky. Our simulated box of 45'^{2} will thus correspond to 9×9 pixels in Planck. Correlations on larger angular scales than 45' will not be available from our simulations. However, the dust correlations will

Frequency [GHz]	100	143	217	353	545	857
$FWHM$ [']	9.5	7.1	5.0	5.0	5.0	5.0
s_X [μKs$^{1/2}$]	32.0	21.0	32.3	99.0	990	45125

increase at smaller angles while the CMB and many other signals will decrease. This means that our lack of information on angular scales $\ell \lesssim 250$ will not be of any consequence, as can be seen in Fig. 4. Planck will measure the CMB at ν = 100, 143, 217, 353, 545, and 857 GHz. We have chosen ν = 353 as our reference frequency. At higher frequencies, the galactic dust will become more of a nuisance and at lower frequencies the CMB primary anisotropies will tend to dominate. To transpose to other frequencies, recall from Eq. 5, that $C_\ell \propto \nu^4$.

In order to test to detectability of the dust with Planck, we evaluate the total error

$$E = \sqrt{\frac{2}{(2\ell+1) f_{cut} L}} \times (E_{CMB} + E_{instrument}), \quad (6)$$

where $f_{cut} = 0.8$ is the percentage of the sky used, L is the binsize, E_{CMB} is the cosmic variance and the instrument error over $\ell(\ell+1)C_l/2\pi$ is

$$E_{instrument} = f_{sky} \frac{4\pi s_X^2}{t_{obs}} \cdot e^{\ell^2 \cdot \sigma_b^2} \cdot \frac{\ell(\ell+1)}{2\pi}, \quad (7)$$

where $f_{sky} = 1$ is the percentage of the sky covered, s_X is the noise per second [μKs$^{1/2}$], $t_{obs} = 14 \cdot 30 \cdot 24 \cdot 3600$ s is the observation time (14 months), and $\sigma_b = FWHM/2.35$ is the lobe sensitivity in radians (FWHM=Full Width Height Median).

For Planck, the values of these parameters are given in table 4.1. The values of the cosmic variance E_{CMB} has been taken from the Lambda web-site: http://lambda.gsfc.nasa.gov (1 March 2005).

The resulting error for a binning of L = 500 along with the dust power spectrum is plotted in figures 4-8. In figure 4, the frequency ν = 353 GHz is fixed while ℓ is varied. We note that $\ell \sim 1000$ seems to be a good place to search for dust. At low ℓ, the error due to the cosmic variance dominates, at high ℓ the instrument noise.

In figures 5 – 8, the binning center is fixed for each figure while the Planck frequencies constitutes the variable. The fourth point in the figures correspond to ν = 353 GHz and apparently gives the best signal over error ratio. At low ℓ the cosmic variance is important, at high ℓ, the instrument error.

4.2. Discussion

The First we compare with SCUBA measurements, see Borys et al. (1999), and find that $\ell(\ell+1)C_\ell^{Dust}/2\pi$ at the mean ℓ = 13081 of SCUBA is $\sim$ 1000 μK^2, see 9, which is much less than $\ell(\ell+1)C_\ell^{SCUBA}/2\pi\big|_{\ell=13081} \approx 55450\ \mu$K^2. This means that the dust signal is too weak to have been detected by SCUBA.

Other detectors that might be of interest are FIRAS II, Fixsen & Mather (2002) BLAST, Devlin (2001) and MAMBO, Greve et al. (2004). BLAST will have a resolution of ~0.5' and a sensitivity which is a factor two lower than SCUBA's. Unfortunately Herschel does not cover the submm frequencies of interest.

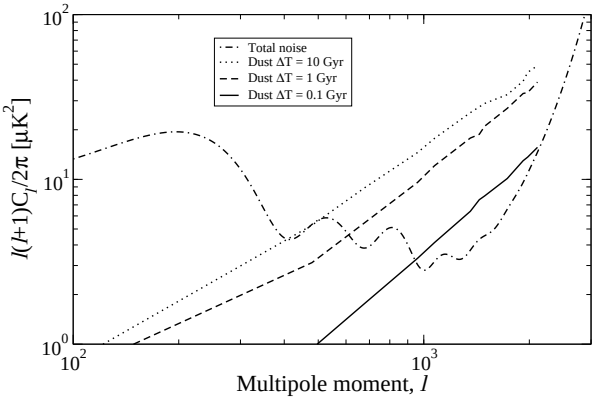

Fig. 4. Comparison between dust power spectrum and Planck error limits at 353 GHz with binning 500. The error limits (total noise) consist of two parts; the CMB cosmic variance, which dominates for small ℓ and the instrument noise, which dominates for high ℓ.

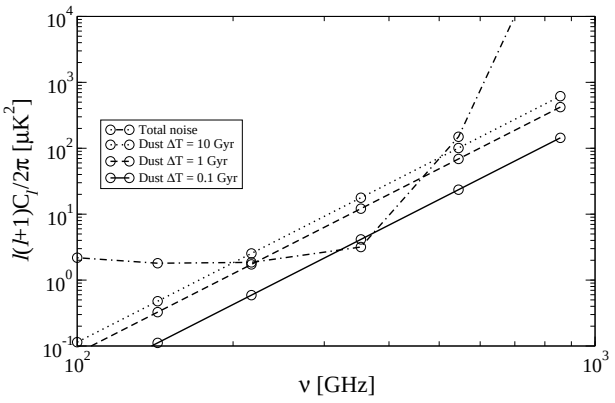

Fig. 5. Comparison between dust power spectrum and Planck error limits at ℓ=1073 with binning 500. The error limits (total noise) consist of two parts; the CMB cosmic variance, which is constant ($\approx$ 1.7) and the instrument noise that has a "U-shape".

As a final remark, we note that other signals that are correlated with structures will also show a similar behavior in the power spectrum.

5. Conclusions

There seems to be a possibility to detect the dust from the first generation of stars with the Planck satellite on small angular scales ($\ell \gtrsim 1000$). However, the detectability depends on the actual distribution of dust in the early universe, but also to a large extent on the dust lifetime. The results are parametrized so that changing the frequency and the fraction of produced metals that become dust is only a matter of scaling the figures. The spectral shape of the early dust is compared to that of the primary CMB anisotropies as well as local dust and found to have a unique signature.

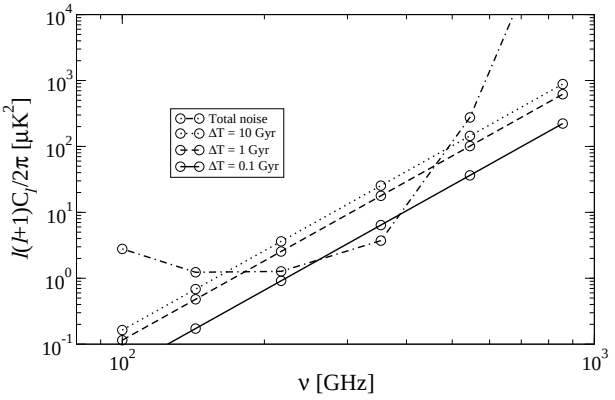

Fig. 6. Comparison between dust power spectrum and Planck error limits at ℓ=1358 with binning 500. The error limits (total noise) consist of two parts; the CMB cosmic variance, which is constant ($\approx$ 1.0) and the instrument noise that has a "U-shape".

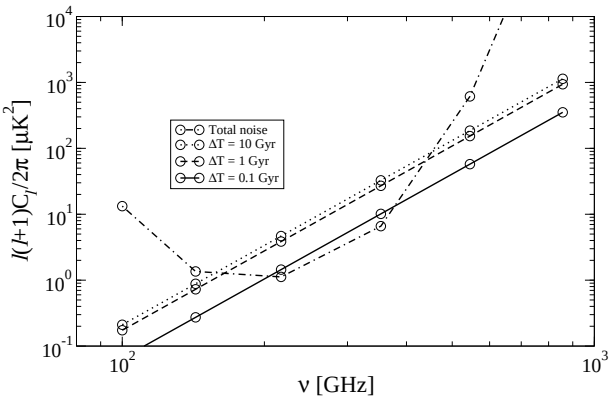

Fig. 7. Comparison between dust power spectrum and Planck error limits at ℓ=1731 with binning 500. The error limits (total noise) consist of two parts; the CMB cosmic variance, which is constant ($\approx$ 0.47) and the instrument noise that has a "U-shape".

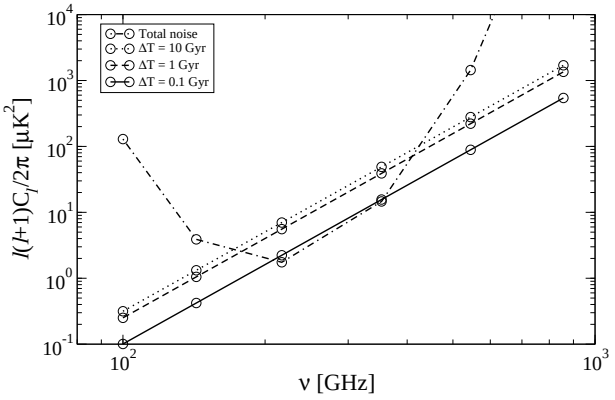

Fig. 8. Comparison between dust power spectrum and Planck error limits at ℓ=2110 with binning 500. The error limits (total noise) consist of two parts; the CMB cosmic variance, which is constant ($\approx$ 0.21) and the instrument noise that has a "U-shape".

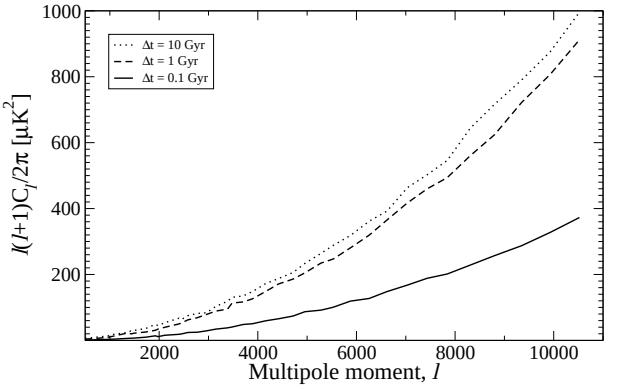

Fig. 9. Dust power spectrum as a function of multipole moment, ℓ, for a map 45'×45' and SCUBA resolution, 1'

References

Bennett, C. L., Halpern, M., Hinshaw, G., et al. 2003, ApJS, 148, 1

Blaizot, J., Wadadekar, Y., Guiderdoni, B., et al. 2003, ArXiv Astrophysics e-prints, astro-ph/0309305

Borys, C., Chapman, S. C., & Scott, D. 1999, MNRAS, 308, 527

Boulanger, F., Abergel, A., Bernard, J.-P., et al. 1996, A&A, 312, 256

Cen, R. 2003, ApJL, 591, L5

Colless, M., Dalton, G., Maddox, S., et al. 2001, MNRAS, 328, 1039

Devlin, M. 2001, in Deep Millimeter Surveys: Implications for Galaxy Formation and Evolution, 59–66

Efstathiou, G. 2003, MNRAS, 343, L95

Eke, V. R., Cole, S., & Frenk, C. S. 1996, MNRAS, 282, 263

Elfgren, E. & Désert, F.-X. 2004, A&A, 425, 9

Fixsen, D. J. & Mather, J. C. 2002, ApJ, 581, 817

Greve, T. R., Ivison, R. J., Bertoldi, F., et al. 2004, MNRAS, 354, 779

Hannestad, S. 2003, Journal of Cosmology and Astro-Particle Physics, 5, 4

Komatsu, E., Kogut, A., Nolta, M. R., et al. 2003, ApJS, 148, 119

Lambda web-site: http://lambda.gsfc.nasa.gov. 1 March 2005

Ninin, S. 1999, PhD thesis: Université Paris 11

Oh, S. P., Cooray, A., & Kamionkowski, M. 2003, MNRAS, 342, L20

Spergel, D. N., Verde, L., Peiris, H. V., et al. 2003, ApJS, 148, 175

Subramanian, K., Seshadri, T. R., & Barrow, J. D. 2003, MNRAS, 344, L31

Szapudi, I., Bond, J. R., Colombi, S., et al. 2001, in Mining the Sky, 249